How to cite: *Angew. Chem. Int. Ed.* **2023**, *62*, e202305323
doi.org/10.1002/anie.202305323

MOF Intersystem Crossing

Triplet Generation Through Singlet Fission in Metal-Organic Framework: An Alternative Route to Inefficient Singlet-Triplet Intersystem Crossing

*Sreehari Surendran Rajasree[+], Jierui Yu[+], H. Christopher Fry, Ryther Anderson, Wenqian Xu, Riya Krishnan, Jiaxin Duan, Subhadip Goswami, Diego A. Gómez-Gualdrón, and Pravas Deria**

Abstract: High quantum yield triplets, populated by initially prepared excited singlets, are desired for various energy conversion schemes in solid working compositions like porous MOFs. However, a large disparity in the distribution of the excitonic center of mass, singlet-triplet intersystem crossing (ISC) in such assemblies is inhibited, so much so that a carboxy-coordinated zirconium heavy metal ion cannot effectively facilitate the ISC through spin-orbit coupling. Circumventing this sluggish ISC, singlet fission (SF) is explored as a viable route to generating triplets in solution-stable MOFs. Efficient SF is achieved through a high degree of interchromophoric coupling that facilitates electron super-exchange to generate triplet pairs. Here we show that a predesigned chromophoric linker with extremely poor ISC efficiency (k_{ISC}) but $E_{S_1} \geq 2E_{T_1}$ form triplets in MOF in contrast to the frameworks that are built from linkers with sizable k_{ISC} but $E_{S_1} \leq 2E_{T_1}$. This work opens a new photophysical and photochemical avenue in MOF chemistry and utility in energy conversion schemes.

Introduction

Achieving a high quantum yield triplets from the initially prepared singlets is key for photocatalytic energy conversion processes.[1] For molecular chromophores—both organic and coordination complex—singlet-triplet intersystem crossing rate can be expressed in terms of their wavefunction overlap as:

$$k_{ISC} = \left(2\pi/\hbar\right)\langle\psi_{T_1}|\hat{H}_{SO}|\psi_{S_1}\rangle^2 f_{FC} \quad (1)$$

Where $\langle\psi_{T_1}|\hat{H}_{SO}|\psi_{S_1}\rangle$ is the spin-orbit coupling (SOC) matrix element and the Franck-Condon factor $f_{FC} = \langle\chi_{T_1}|\chi_{S_1}\rangle^2$; here ψ and χ are the electronic and vibrational wavefunctions, respectively.[2] For such spin-forbidden non-adiabatic transitions impressive k_{ISC} can be achieved through a sizable SOC facilitated by heavy atoms (i.e., the Z_{eff} term in the $\hat{H}_{SO}$) and proper orbital configuration and spatial overlap.[2a,b,3] Whereas the f_{FC} follow the energy gap law:[4] in the weak coupling limit, for "matching" potential energy surfaces, $f_{FC} \propto \exp(-\Delta E_{ST})$, and will involve a reorganization energy for non-matching surfaces with unequal electronic structure.[2a–c,3b,5] Disparate spatial extent of the singlet and triplet wavefunctions,[6] therefore, will lead to a diminished f_{FC} between them causing a non-detectable triplet (T_1) yield.[7] Excitonic coupling among the molecular units within chromophore assemblies dictates the extent of the spatial distribution of the excitonic center of mass, which may scale differently for their singlet and triplet excitons.[8] While such a phenomenon is well established in (covalently linked) macromolecules, oligomers, and/or polymers, it is not well studied in their non-covalent solid assembly such as organic crystal, and porous frameworks.[6–9]

Metal–organic frameworks (MOFs) are emerging porous materials with unique photophysical properties suitable for energy conversion.[10] Such porous pigment/linker assemblies can be perceived to generate a high triplet population via efficient ISC facilitated by the heavy metal ions (such as Zn^{2+}, Zr^{4+}, etc.) present at their interconnecting node. However, it was not well established if such perception is generally true other than those constructed from linkers that possess directly accessible ^{3}MLCT state (seen in, for example, $Ru(bpy)_3^{2+}$ based MOFs[10c,11]).

[*] S. Surendran Rajasree,[+] J. Yu,[+] R. Krishnan, Prof. Dr. P. Deria
School of Chemical and Biomolecular Sciences, Southern Illinois University Carbondale, 1245 Lincoln Dr., 62901 Carbondale, IL (USA)
E-mail: pderia@siu.edu

R. Anderson, Prof. Dr. D. A. Gómez-Gualdrón
Department of Chemical and Biological Engineering, Colorado School of Mines, 1500 Illinois St, 80401 Golden, CO (USA)

Dr. H. C. Fry
Center for Nanoscale Materials, Argonne National Laboratory, 9700 S Cass Ave, 60439 Lemont, IL (USA)

Dr. W. Xu
X-ray Science Division, Advanced Photon Source, Argonne National Laboratory, 9700 S Cass Ave, 60439 Lemont, IL (USA)

J. Duan, Dr. S. Goswami
Department of Chemistry, Northwestern University, 2145 Sheridan Road, 60208 Evanston, IL (USA)

[+] These authors contributed equally to this work.

In our previous works, we have established that the singlet excitons in MOFs are spatially dispersed over multiple linkers for a variety of Zr^{4+}-oxo-based frameworks constructed from organic linkers made with pyrene, phenyl-ethynyl-phenyl, and porphyrin cores—this model effectively describes the singlet exciton hopping.[12] Here we show that such framework assemblies suppress the singlet→triplet ISC despite being constructed from triplet-producing linkers (with sizable triplet population, Φ_{ISC}, in their solution-dissolved phase) and heavy metal ions-based node (Figure 1). Circumventing such sluggish ISC, here we show that singlet fission (SF)[13] can be a viable route to achieve high quantum-yield triplets in MOFs.

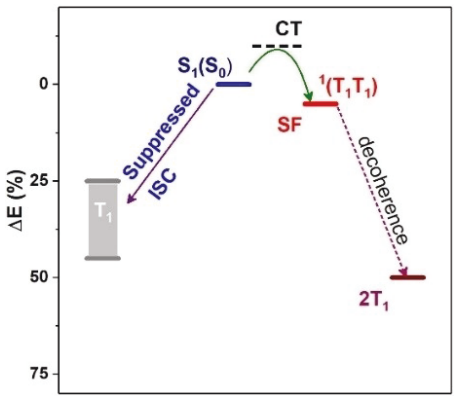

Figure 1. Energy diagram for singlet→triplet conversion in chromophore assemblies in MOFs highlighting a suppressed ISC for a system where $\Delta E_{ST} < 50\%$ of E_{S_1}. A larger triplet population can be achieved via singlet fission for linkers with $\Delta E_{ST} \gtrsim 50\%$ of E_{S_1} via electronic exchange involving a virtual CT state.

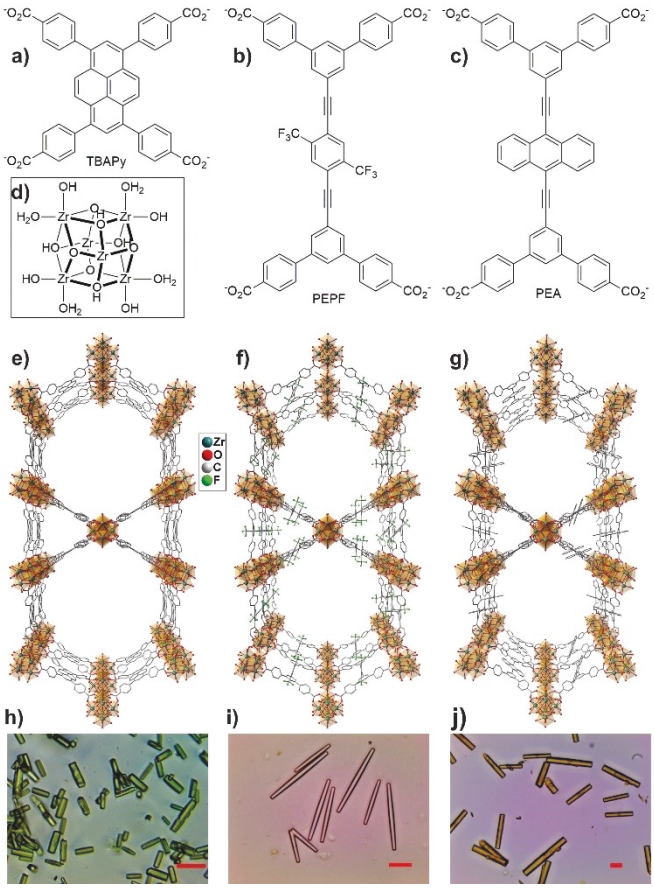

Figure 2. Structure of the a) TBAPy, b) PEPF, and c) PEA linkers and their (d) Zr_6^{IV}–oxo based MOF (e) NU-1000, f) SIU-100, and g) SIU-175. Lower panels (h–j) display corresponding optical microscopic images (scale bar: 50 μm).

In this study, we take three chromophoric linkers with diverse chemical and electronic symmetry built from rigid pyrene core and Ph–E–Ar–E–Ph (E = ethynylene, Ar = aromatic core) backbone such that they differ in their respective ΔE_{ST}. For tetraphenylpyrene (TBAPy), and 1,4-bis(ethynylene phenyl)-2,5-bis(trifluoromethyl)phenyl-derived PEPF linkers (Figure 2), the $\Delta E_{ST} \lesssim 0.45\%$ of their initially generated S_1 energy (E_{S_1}).[14] When the central aromatic component in the Ph–E–Ar–E–Ph core is replaced with anthracene, the resulting 9,10-bis(ethynylene phenyl)anthracene[15] derived PEA linker possesses $\Delta E_{ST} \gtrsim 0.50\%$ of its E_{S_1}. This feature fulfils the energetic requirement for SF—we show that PEA based MOF, SIU-175 (Figure 2), can produce sizable triplet population. The new MOF, SIU-175(***xly***) has a comparable structure to NU-1000 (***csq***) and SIU-100 (***xly***) with similar inter-linker orientation within their assemblies.

Results and Discussion

Photophysical properties, probed via various steady-state and time-resolved spectroscopic methods, suggest that the TBAPy, PEPF, and PEA linkers have high fluorescence quantum yield ($\Phi_{em} \gtrsim 80\%$ in their dilute solution with a single component time constant (Figure 3; Table 1). TBAPy linker forms triplet with a weak low-temp phosphorescence ($\approx$670 nm);[16] nanosecond transient absorption (ns-TA) spectra and the corresponding kinetics recorded in deaerated 2-methyl tetrahydrofuran (MeTHF) solvent show a weak $T_1 \rightarrow T_n$ transition at ≈400–600 nm that persist over 20 μs and can be quenched by oxygen ($\tau \approx 50$ ns; Figure 3a–c; and Figure S14). In contrast, TBAPy assembly in NU-1000 (Figure 2a, e) does not manifest any sizable triplet population from its initially generated singlets (λ_{ex} = 355–400 nm);

Table 1: Emission Lifetime Data for TBAPy and PEPF linkers and their MOF Samples.

Compound	Φ_{em}	τ_{S1} [ns]	τ_T [μs][b]
Et_4TBAPy	80%	1.9	>20 (0.05)
NU-1000	47% (47%[a])	1.0 (0.95[a])	–
Et_4PEPF	80%	3.2	11 (0.10)
SIU-100	37% (39%[a])	0.85 (0.84[a])	–
Et_4PEA	98%	2.56	–
SIU-175	39% (17%[a])	0.25; 3.0; 11.3 (0.1, 1.2, 6.5[a])	1.2×10^{-3}

Data collected at RT, argon ([a] air purged media), MeTHF solvent; error manifested in $\Phi_{em} = \pm 2\%$ and in time constants ±0.05 ns. See Figures 3 and S14–16 for spectra. [b] Measured from ns-TA experiments.

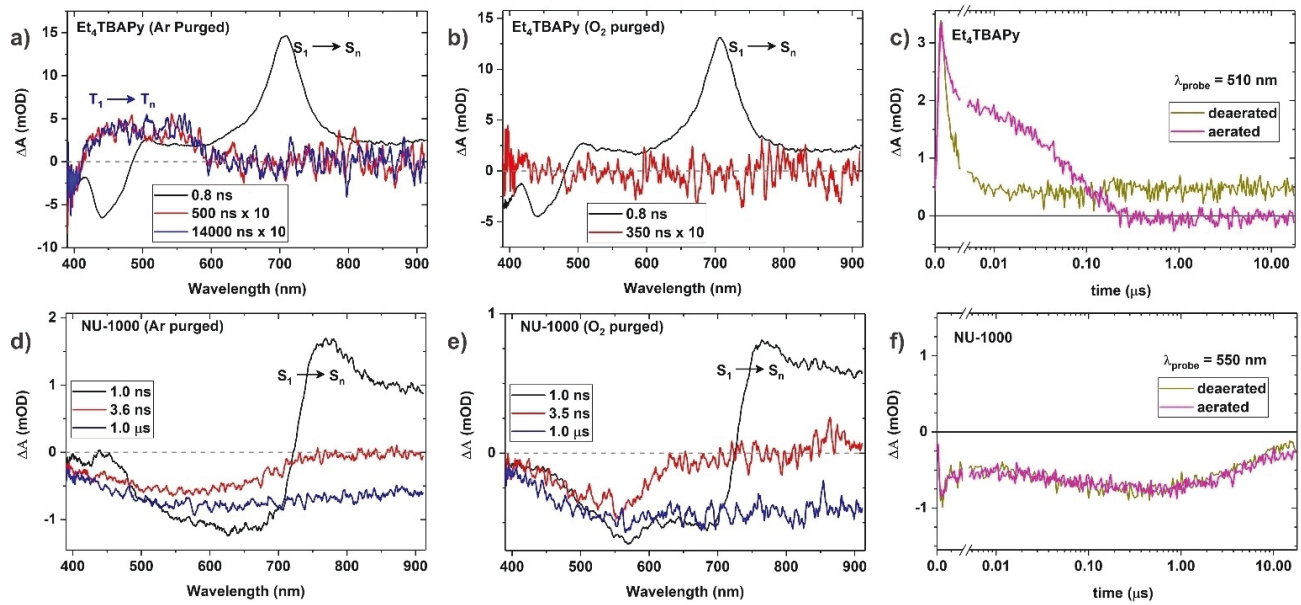

Figure 3. Nano-second TA spectra of unassembled (a–c) Et_4TBAPy linker (ester form) showing weak but long-lived T_1-T_n absorptions in (a) deaerated MeTHF solvent that is quenched in (b) the corresponding aerated solvent; (c) corresponding kinetic profiles. Oxygen insensitive ns-TA spectral feature for (d–f) NU-1000 showing the early $S_1 \rightarrow S_n$ absorption and broad excimer ($\approx$5 ns) leading to a broad, long-lived, featureless negative signal, which stems from various singlet complexes See Supporting Information sec E2 for further detail.

the ns-TA spectra and the corresponding kinetics are mostly insensitive to molecular oxygen.[17] These ns-TA spectra for NU-1000 are highlighted by an early signature of a singlet population with ground-state bleaching (GSB) and stimulated emission (SE) in 400–650 nm, and $S_1 \rightarrow S_n$ transition at $\approx$750 nm. These signatures disappear within a few ns ($\tau \approx 1$–2 ns) and a weak broad signal (600–1000 nm) appears for their excimer-like complex.[12a,18] In the longer time delay a featureless broad bleaching signal dominates over several microseconds (which is insensitive to O_2 and stems from various excited state complexes; see Supporting Information sec E3 for details). Similar ns-TA spectra collected for PEPF and its MOF assembly SIU-100 (Figure 2b, f) can be found in Figure S14.

A suppressed ISC in Zr MOFs like NU-1000 and SIU-100, (Figure S14) with no detectable triplet spectral feature is counterintuitive from the perspective of its heavy-metal connected assembly expected to boost the ISC. Particularly, when both the TBAPy and PEPF linkers display the formation of their respective long-lived triplets in the solution phase. We postulate that this is due to different extents of spatial dispersion of their singlet (delocalized) and triplet (localized) excitons. We have shown, in our previous studies, through TDDFT computations with small models of linker assembly (constructed from their crystallographic coordinates; see Supporting Information-D1) that the singlet excitons span over three linkers of their triangular assembly.[12a,c] Corresponding transition density matrix (TDM) analyses, however, highlight a single-linker localized triplet exciton (Figure 4; see Figure S7 for higher energy triplets)—such disparity, therefore, causes poor Φ_{ISC}. These results reason well why the triplet studies in MOFs, constructed from aromatic pigment-based linkers, are limited by triplet sensitization via Dexter energy transfer using platinum porphyrin/phthalocyanine.[16,19]

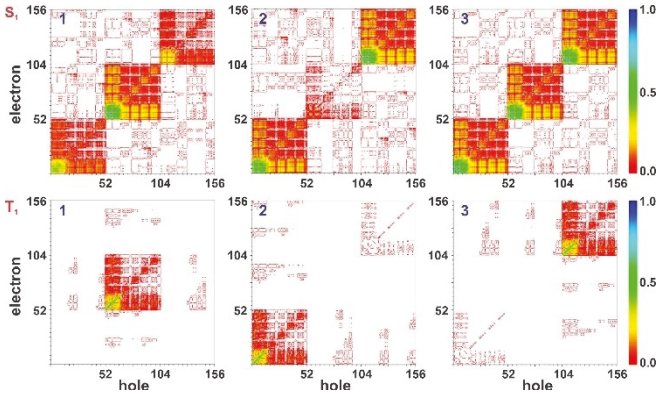

Figure 4. Contour plots of TDMs for (top row) three excitonic states in the S_1 manifold (two dark, one bright, evolved from the first excited state of three linkers) computed for a triangular H_4TBAPy assembly (see Figure S7) in NU-1000. The lower panel represents the corresponding three lowest energy triplet excitonic states of the T_1 manifold highlighting a localized system. Computation: cam-b3lyp/6-31 g(d,p); the color bars represent the normalized atomic transition densities. See Supporting Information sec D1 for details.

The 9,10-bis(ethynylene phenyl)anthracene core of the PEA linker is known to possess poor k_{ISC} with no detectible phosphorescence in its dilute solution.[15] TDDFT computation of H_4PEA provides $E_{S_1} \approx 2.43$ eV and $E_{T_1} \approx 1.18$ eV. The $E_{T_1} \approx 0.5 \times E_{S_1}$ is maintained in other rotational conformation (see Supporting Information sec D2); e.g., for a conformation where anthracene is rotated by 45° relative to the four carboxylates caused a rise of the E_{T_1} to *ca*

1.23 eV—where the singlet energy is also being raised (2.55 eV). To exploit the SF as a feasible route in generating high quantum yield triplets, the PEA linker was assembled in SIU-175 yielding anisotropic needle-shaped crystals (Figure 2j) which is typical of *csq*/*xly* topological nets (like, NU-1000, PCN-222, SIU-75, and SIU-100, etc.) prepared under thermodynamically controlled conditions at relatively higher temperatures. The structure of the SIU-175 was determined via Rietveld fitting of powder synchrotron diffraction (PSRD) data collected for solvent-soaked MOF samples (Figure 5; CCDC No: 2216519).[20] Much like other frameworks made with anisotropic and flexible linkers,[12b,21] SIU-175 displays a capillary-force-driven pore shrinkage upon removal of the occupied solvents (Figure S3) reporting a residual porosity with a BET surface area of 200 $m^2 g^{-1}$ (N_2 isotherms at 77 K; Figure S5), where the experimental pore size distribution (N_2 isotherm), matches, with the computationally predicted pore size patterns.[22] Maintaining the structural integrity of such a low-density framework during all the spectroscopic works, the MOF samples were stored and manipulated under solvent-soaked conditions (i.e., samples were prepared by solvent exchange).

Given both the triangular micropore and hexagonal mesopore would provide a range of the rotational population in PEA linkers, we wanted to verify their relative orientation—possibly dictated by the steric hindrance and strain imparted by the SIU-175 assembly—ensuring the energetic criteria (see Supporting Information sec D2 for details of linker torsional arrangements). Systematic optimization of the relative rotational conformations of three PEA linkers within a small model provided a structure (Figure S11) that could describe the experimental absorption spectra (Figure 6a; Figure S12)—which is sensitive to the anthracene rotational conformation and excitonic interactions. The TDDFT results with such model arrays confirmed the maintenance of $E_{S_1} \approx 2E_{T_1}$.

The Steady-state excitation-emission mapping spectra (EEMS) for Et_4PEA (Figure 6b) highlights the lowest energy excitation/emission manifolds centered at 450/482–550 nm ($\Phi_{em} \approx 98\,\%$) with a well-resolved vibronic spectral envelope: υ_{0-0} (482 nm), υ_{0-1} (515 nm), and υ_{0-2} (550 nm)

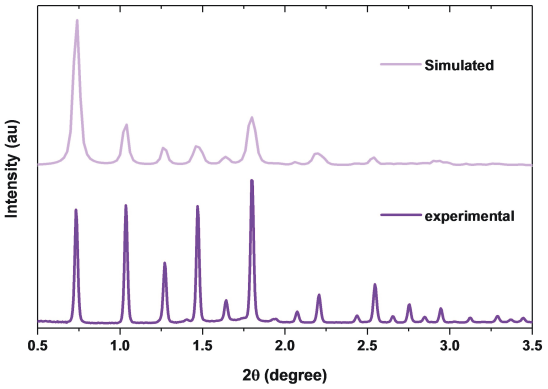

Figure 5. PSRD patterns collected for DMF-soaked SIU-175; The simulated pattern, obtained from Rietveld modeling, shows a good agreement with the experimental pattern.

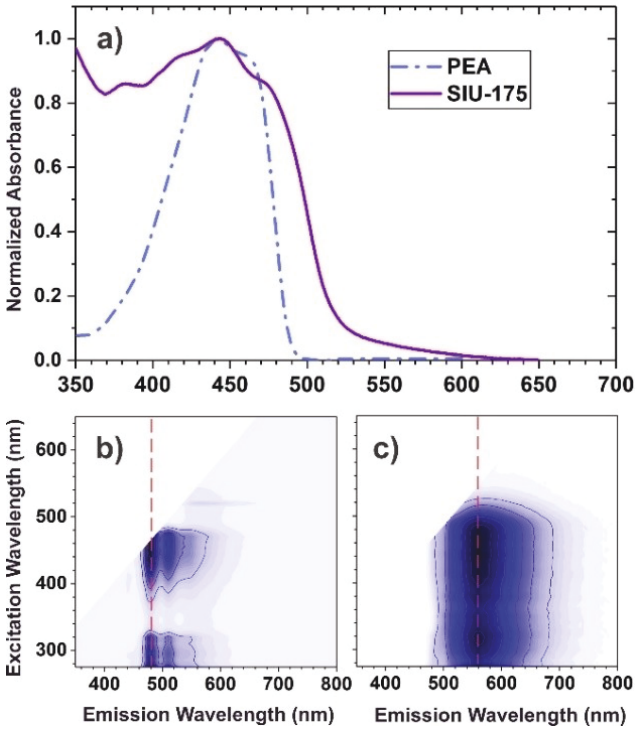

Figure 6. (a) Absorptive electronic transitions of SIU-175 (violet) along with the H_4PEA linker (dashed, blue). (b) Excitation-emission mapping spectra (EEMS) of Et_4PEA (≈0.4 μM), and (c) SIU-175 collected in deaerated MeTHF solvent (RT; dark blue area represents the most intense signal).

transitions. Like its core component, Et_4PEA did not display any detectible phosphorescence, indicating a poor Φ_{ISC} ($\lesssim 10^{-5}$).[23] In contrast, the EEMS plot for SIU-175 peaks around 475/565 nm (FWHM ≈ 3203 cm^{-1})—with an overall $\Phi_{em} \approx 39\,\%$. Such broad spectral envelop can stem from unresolved emission lines originating from an excimer like complex (S_{exc}),[18] or delayed emission from a low-energy state (denoted as S_l). The latter involves population via triplet-triplet annihilation (TTA). Time-resolved emission spectroscopic data (TRES; Figure 7) suggest that SIU-175 produces narrow spectra at the earlier time (FWHM = 1750 cm^{-1} measured at 0.05–0.1 ns) peaking at 525 nm (with a 550 nm shoulder) and broadband, centered at 560 nm (with 510 and 550 nm shoulder), appears late (FWHM = 3250 cm^{-1} measured at 1 ns). Global fitting of the transient kinetic profiles provided three time constants (Table 1): a fast $\tau_1 \approx 0.25$ (±0.05) ns and the $\tau_2 \approx 1$ ns components can be assigned to shorten S_1 state lifetime (compared to a single component 2.56 ns time constant for Et_4PEA in its dilute solution) associated to efficient formation of other states and energy transfer (transporting the excitons from the outer sites of the crystals). The longer time constants ($\tau_3 \approx 11$ ns) can be assigned to a delayed formation of a low energy state (displaying an $S_l \rightarrow S_0$ emission)—this can be visualized by wavelength-dependent transient emission profiles (Figure 7).

To glean deeper into the origin of this delayed emission, triplet quenching experiments were carried out: SIU-175 in

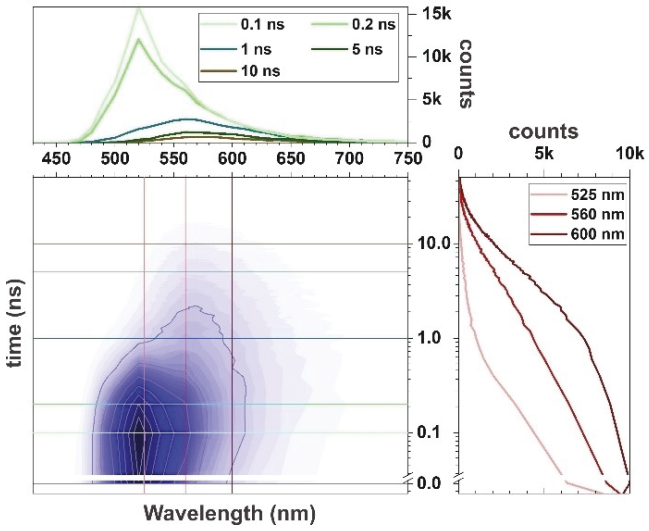

Figure 7. TRES plot for SIU-175 in MeTHF solvent ($\lambda_{ex}=403$ nm; 298 K; dark blue area represents the most intense signal). The respective transient emission spectra at labeled time delays are shown at the top panels and representative transient kinetic profiles probed at labeled wavelengths are presented at the right panel.

the presence of O_2 display a staggering ≈50 % loss in the emission quantum yield (Table 1) due to the quenching of the broad low-energy emission (Figure 8; S15). This indicates that the delayed low-energy emission is associated with

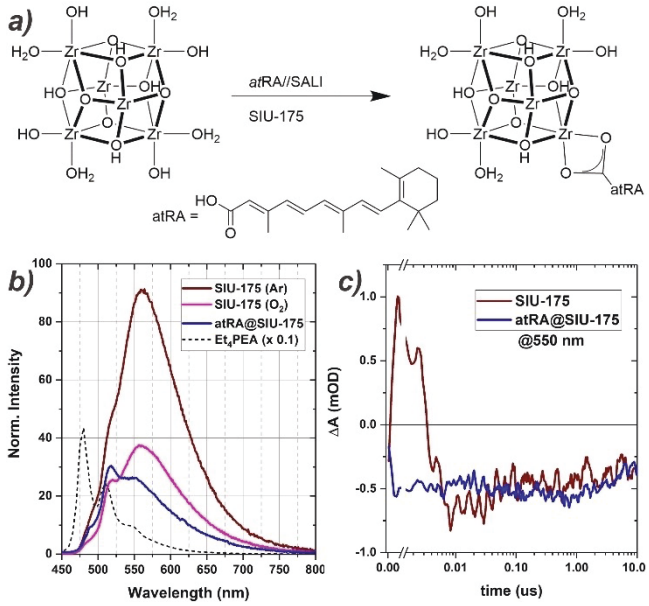

Figure 8. a) Solvent Assisted Linker Incorporation (SALI) installation of *at*RA at the 8-connected Zr_6-oxo node of the mesoporous SIU-175 (≈1 *at*RA/node). (b) Quenching of delayed fluorescence in SIU-175 (through re-population by the triplets via TTA) by molecular oxygen (pink) and by node-installed *at*RA (violet) in *at*RA@SIU-175; and (c) the ns-transient kinetic profiles probed at 550 nm highlighting the quenching of the triplet population in atRA@SIU-175 ($\lambda_{ex}=355$ nm; pump fluence = ≈680 μJ/cm^2; MeTHF; 298 K).

triplets in the PEA assembly of SIU-175. Given a staggering ≈50 % QY loss (at room temperature), with $E_{S_l} \approx 0.9 \times E_{S_1}$, the low-energy state cannot possibly be a triplet by itself but a singlet that is evolved from triplets via TTA.

To further probe such triplet quenching, circumventing any argument related to the efficiency of diffusion (molecular O_2 and triplet excitons) within these molecular scale pores of SIU-175, as well as other quenching mechanism involving an oxygen adduct and/or radical ions, a node-installed low-energy triplet quencher was exploited. Energetically all-*trans*-retinoic acid (*at*RA) is a good candidate as a triplet quencher given its high energy S_1 state (absorption peak of ≈350 nm, ensuring *at*RA cannot serve as a singlet energy acceptor from S_1 of SIU-175) where its low-lying T_1 (≈1.2 eV) is well aligned with that of the PEA (see Supporting Information-sec G, Figure S22). The carboxy-terminated *at*RA was installed at the 8-connected Zr-oxo node of the SIU-175 via SALI chemistry (Figure 8a).[10f,g,24] The emission profile and QY data collected for the *at*RA@SIU-175 are consistent with the O_2 quenching experiment (Figure 8b) with overall $\Phi_{em}=14$ %. The emission line highlights a quenching of the low-energy $S_l \rightarrow S_0$ emission line (Figure 8b) Such quenching is corroborated by a faster emission decay seen in the TCSPC profile of the *at*RA@-SIU-175 relative to the pristine SIU-175 MOF (Figure S15, S23). The corresponding ns-TA kinetic data (MeTHF solvent; Figure 8c) highlights a complete quenching of the initial signal seen in the pristine SIU-175 except for a leftover broad bleaching signal also seen in other MOF samples like in NU-1000 that possess high energy singlet state (See Supporting Information sec E3 for details).[25]

These data unambiguously suggest an efficient formation of triplets in PEA-assembly in SIU-175 (compared to other related Zr-MOFs like NU-1000 and SIU-100) and their efficient TTA-driven delayed formation of the emissive S_l state. To investigate the dynamics of the SF process and elucidate a possible mechanism, femtosecond transient absorption (fs-TA) spectroscopic investigations were carried out. As expected, the Et_4PEA ($\lambda_{ex}=450$ nm; MeTHF; 298 K) manifest singlet excited state (Figure S13) highlighted by an excited-state absorption (ESA) band for $S_1 \rightarrow S_n$ transitions at 530–750 nm, GSBat 460 nm, and SE at ≈515 nm. The singlet state monotonously decays with time constant $\tau=2.26$ ns without any detectable triplet signature (see Table 1 for comparison).

In contrast, the fs-TA spectra for SIU-175 ($\lambda_{ex}=425$ nm, MeTHF; Figure 9) highlight the evolution of multiple transient species. At early time delays, the ESA bands—one peaking at *ca* 640 nm and the other broad intense band at *ca* 1150 nm—highlight $S_1 \rightarrow S_n$ transitions, which can be seen along with the GSB at 480–500 nm and a SE at 550 nm. Based on the singular value decomposition (SVD) analyses, the fs-TA data were globally fit with a two-species sequential target model—i.e., $\mathbf{A} \rightarrow (k_1) \rightarrow \mathbf{B} \rightarrow (k_2) \rightarrow$gs (eqs: 2–3; branched recombinations of these excited state species are inefficient and therefore, their decay can be effectively modeled by a sequential model; see Supporting Information sec F; for details):

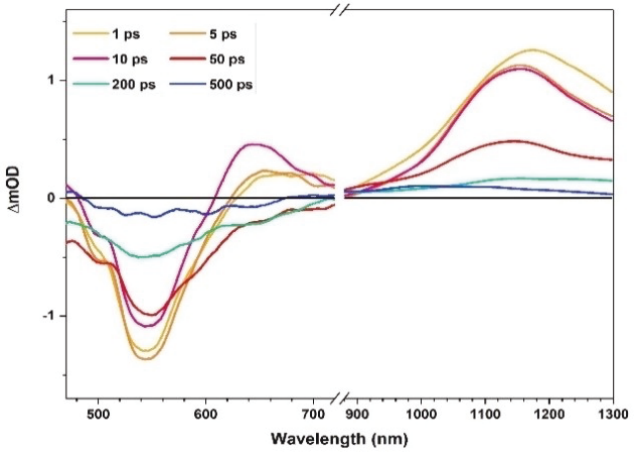

Figure 9. Representative fs-TA spectra for SIU-175 suspension in MeTHF solvent at labeled delay times. Experimental condition: λ_{ex} = 425 nm; fluence ≈ 280 μJ/cm^2.

$$\frac{d[A]}{dt} = -k_1[A] \tag{2}$$

$$\frac{d[B]}{dt} = k_1[A] - k_2[B] \tag{3}$$

In general, the initial singlet species (i.e., a singlet pair, S_1S_0) decays to an SF intermediate (i.e., a triplet pair, ^{1}TT), which then forms triplets (eq 4). However, the detection of the intermediates—i.e., assignment of their respective species associate spectra (SAS)—can be limited by the instrumental resolution depending on the corresponding dynamics.

$$[S_1S_0] \xrightarrow{k_{SF}} {}^1(T_1T_1) \xrightarrow{k_{decoh}} 2T_1 \tag{4}$$

Here, k_{SF} is the rate constant for the spin-allowed SF process and depends on the extent of electronic superexchange coupling $\langle S_1S_0|\hat{V}|T_1T_1\rangle$ between the initial singlet and correlated triplet pair states. The SAS (Figure 10) of the initial species **A** is highlighted by an intense SE at 550 nm along with a GSB at ≈500 nm. While two ESA peaks corresponding to $S_1 \rightarrow S_n$ transitions indicate species **A** being the initial singlet pair, the intense SE signifies an unresolved signature of the ^{1}(TT) pair formed via an efficient SF process. Examination of the fs-TA spectra at early time delays (Figure 9) suggests that this SE peak appears < 1 ps and decays faster than the GSB recovery, which corroborates with its assignment to ^{1}(TT).[26] The GTA analysis suggests that the SAS of **A** decay to **B** with $k_1 = (41\ \text{ps})^{-1}$. Species **B** (Figure 10) has a lifetime of $\tau = 1.2$ ns, and population dynamics suggest that ≈90 % of the initial **A** forms **B**. Congruent with the ns-TA spectra and quenching experiment (Figure 8, Supporting Information-sec G), species **B** can be assigned to the triplets and its 1.2 ns lifetime is consistent with the efficient TTA process generating low-lying singlet state (delayed emission with $\tau \approx 10$ ns; see above). The excited state dynamical processes are summarized in Figure 11.

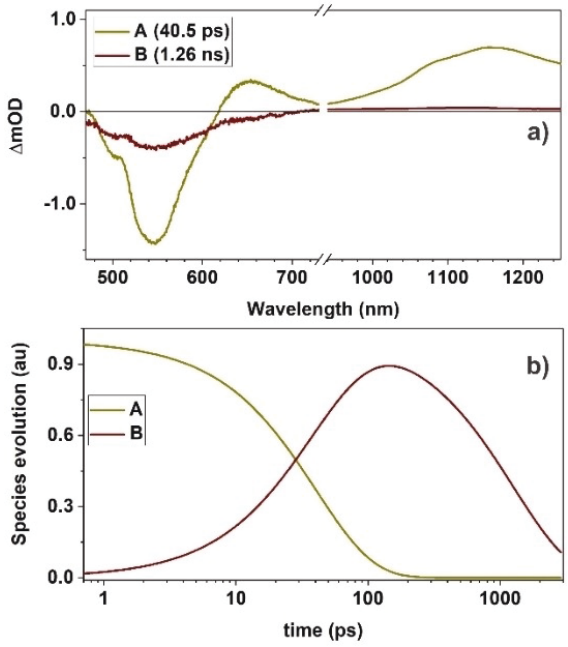

Figure 10. a) Plots of SAS generated from GTA model fit of the fs-TA data for SIU-175 in MeTHF solvent; b) Corresponding population dynamics are shown in the lower panels.

The sensitized triplet generation was explored to characterize its spectral signature. For efficient sensitization via Dexter energy transfer, a carboxyphenyl appended palladium tetraphenylporphyrin was used to install at the Zr node (≈0.05 TPP(Pd)/PEA; see Supporting Information sec G2). In the sensitized ns-TA experiment, a selective excitation (λ_{ex} = 532 nm; red to PEA absorption) of TPP(Pd) moiety manifested a spectral signature that appeared to be comparable to the SAS of species **B** generated by a direct

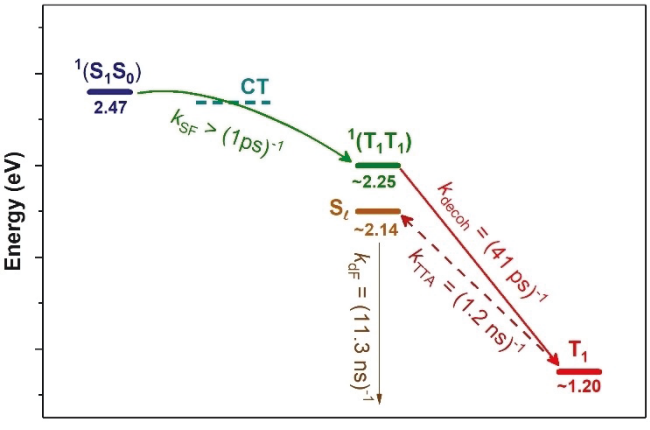

Figure 11. Energy diagram describing the dynamics of the excited state species associated with the SF process. The rate constants for the decoherence, TTA, and delayed fluorescence are for those measured in MeTHF solvent, in CF_3Tol solvent they are (26 ps)$^{-1}$, (2.5 ns)$^{-1}$, and (7.3 ns)$^{-1}$, respectively.

355 nm excitation of the pristine MOF (Figure S25). It is important to note, however, that the sensitized triplet spectrum lacks the ESA signal (>600 nm) that remained unresolved in the SAS of Species **B** (obtained via high-energy singlet excitation 355 nm) of pristine MOF (Figure S25).[15,27]

Given that the carboxy-coordinated Zr^{IV} (at the node) does not manifest any sizable impact facilitating a singlet-triplet ISC in linker assemblies like NU-1000, and SIU-100 (Figure 3, Figure S13), it is important to elucidate the proposed SF route in the PEA assembly in SIU-175 a bit deeper. SF pathway[28] has been described to proceed through an electron super-exchange process[29] that involves a charge-transfer (CT) virtual state. A photophysical probe at a different dielectric medium was made possible by infiltrating the pores of this solution-stable framework with the desired solvent. A relatively polar solvent, e.g., CF_3Tol ($\varepsilon = 9.2$) can stabilize the CT state and, therefore, facilitate the SF: analysis of the fs-TA spectral data of SIU-175 collected in CF_3Tol solvent (Figure S26) evinced a faster formation of species **B** with $k_1 = (26\ \text{ps})^{-1}$ compared to that observed in MeTHF solvent ($k_1 = (40\ \text{ps})^{-1}$; Figures 10–11, see above). Species **A**, in CF_3Tol solvent, also displayed an intense SE signal from the unresolved ^{1}(TT). Furthermore, SIU-175 manifested a small Φ_{em} ($\approx 23\,\%$) with an emission profile that appears like the one upon O_2 quenching profile (Figure S27). This indicates a suppressed TTA process involves a polar state(s). The ns-TA data recorded in CF_3Tol solvent suggested slightly longer-lived triplets (2.5 ns compared to the 1.2 ns time constant measured in MeTHF solvent; Figures S21, S26).

To further check if the delayed low-energy emission was indeed stemming from the TTA process,[16,19,30] TPP(Pd)@SIU-175 was examined at multiple excitation wavelengths. Excitation at 480 nm manifested a direct linker-based emission with a well-resolved set of vibronic bands appearing at 510 nm and 550 nm, and a low energy band at 580 nm (Figure S26).[31] Selective excitation at 528 nm, however, yielded the 580 nm peak without much of the 550 nm band. Exiting further red ($\lambda_{ex} = 580$ and 600 nm), the TPP(Pd) based fluorescence ($S_1 \rightarrow S_0$ at 610 nm) and phosphorescence ($T_1 \rightarrow S_0$ at 655 and 710 nm) appeared to dominate the emissive profile, but with the notion of 580 nm peak from the framework without the 510 and 550 emissions.

Conclusion

Achieving high quantum yield triplets, populated by initially prepared singlets, is desired for various energy conversion processes in solid working compositions like MOFs. However, the disparate spatial distribution of the excitonic center of mass results in a diminished Franck-Condon overlap, leading to a poor singlet-triplet intersystem crossing efficiency (k_{ISC}) in such solid assemblies despite being constructed from a carboxy-coordinated zirconium heavy metal ion (supposedly improve SOC matrix element). Circumventing this sluggish ISC, singlet fission (SF) is explored as a viable route to generating triplets. Efficient SF is achieved through a high degree of interchromophoric coupling that facilitates electron super-exchange to generate triplet pairs. Here we show that a predesigned chromophoric linker with $E_{S_1} \geq 2E_{T_1}$ and extremely poor k_{ISC} (in dilute solution) indeed produce triplets when assembled in MOF. In contrast, similar MOF structures that were prepared from linkers with $E_{S_1} \leq 2E_{T_1}$ do not form any detectable triplets despite a good k_{ISC} of the corresponding linker. Examining two electronically distinct linkers (TBAPy and PEPF) and their structurally comparable frameworks as control systems, we underpin that a wavefunction mismatch between their spatially dispersed singlet and localized triplet excitons could lead to a poor k_{ISC} in their MOF assemblies. The TBAPy and PEPF (with $E_{S_1} \leq 2E_{T_1}$) in their dilute solution manifest long-lived triplets that can be quenched by molecular oxygen. In contrast, their assemblies in MOF display O_2-insensitive excited-state dynamical features. This is intriguing given that the frameworks were constructed by interconnecting the linkers with Zr^{IV}—based nodes through carboxy bonds. This study suggests that the spin-orbit coupling of such heavy metal ions cannot facilitate the ISC in these organic pigment/linker assemblies.

For SF, an organic pigment populates its triplets through a process that requires a macromolecular or supramolecular assembly hosting two pigment cores in proximity. For this, the $E_{S_1} \geq 2E_{T_1}$ must be satisfied. In this study, 9,10-bis(ethynylene phenyl)anthracene PEA linker was assembled into SIU-175 having a topological (*xly*) net that is comparable to the NU-1000 and SIU-100. Unassembled PEA in dilute solution does not have a sizable triplet population; in contrast, its assembly in SIU-175 facilitates electronic interaction that leads to generating triplet pairs through a virtual electron super-exchange process. The ultrafast transient spectroscopic study suggests efficient SF within 1 ps followed by decorrelation generating quenchable triplets with a rate constant of $(41\ \text{ps})^{-1}$. These triplets, due to a large triplet population and sizable triplet diffusion, can repopulate a low-energy singlet state (S_1) via triplet-triplet annihilation (TTA). While the scattering nature of our sample hinders an exact estimation, the large extent of (TTA-derived) delayed emission with an intrinsic $\approx 15\,\%$ radiative decay and analyses of the TA-dynamics, an upper limit of $\approx 170\,\%$ triplet population can be expected in SIU-175.

In the context of energy conversion schemes, like photochemical and photoelectrochemical systems, SF in MOF will provide a solid platform to improve quantum efficiency by generating $>100\,\%$ excitons, where a solution stable framework could host a series of beneficial features (like selective substrate/product diffusion, accessible complementary redox moieties, dielectric modulation, and so on). Such developments must, however, be carried out carefully as the potential energy of the generated charges from these low-energy triplets may be a limiting factor to drive some demanding transformations. The periodic assembly of chromophores around the well-defined pores also provides structural "rigidity" and the opportunity to modulate topology to establish structure–property relationships. While these factors can be great assets for precisely tuning the

desired properties compared to say a polymer immobilized system, the energy landscape in MOF systems will be defined and limited by the pore geometry (shape and size) in a way that a compact assembly may not be possible and that the timescale to utilize the triplets would be limited by parasitic TTA process that cannot be completely suppressed in these periodic systems hosting highly mobile excitons.

Acknowledgements

P. D. gratefully acknowledges funding from the National Science Foundation (NSF CAREER CHE-1944903). D. A. G.-G. thanks for support from the NSF CAREER Award (CBET 1846707) and computational resources from Colorado School of Mines (Mio Supercomputer). Work performed at the Center for Nanoscale Materials, a U.S. Department of Energy Office of Science User Facility, was supported by the U.S. DOE, Office of Basic Energy Sciences, under Contract No. DE-AC02-06CH11357. This research used Beamline 17-BM of the Advanced Photon Source; a U.S. Department of Energy (DOE) Office of Science User Facility operated for the DOE Office of Science by Argonne National Laboratory under Contract No. DE-AC02-06CH11357. J. D. and S. G. acknowledge the support from the U.S. Department of Energy, Office of Science, Office of Basic Energy Sciences via grant DE-FG02-87ER13808.

Conflict of Interest

The authors declare no conflict of interest.

Data Availability Statement

The data that support the findings of this study are available in the supplementary material of this article.

Keywords: Crystalline Assembly · Inhibited ISC · Singlet Fission · Triplets · Zr-MOF

[1] a) T.-Y. Shang, L.-H. Lu, Z. Cao, Y. Liu, W.-M. He, B. Yu, *Chem. Commun.* **2019**, *55*, 5408–5419; b) T. Koike, M. Akita, *Inorg. Chem. Front.* **2014**, *1*, 562–576; c) J. I. Goldsmith, W. R. Hudson, M. S. Lowry, T. H. Anderson, S. Bernhard, *J. Am. Chem. Soc.* **2005**, *127*, 7502–7510; d) F. Strieth-Kalthoff, F. Glorius, *Chem* **2020**, *6*, 1888–1903.

[2] a) N. J. Turro, *Modern Molecular Photochemistry*, University Science Books, Sausalito, **1978**; b) C. M. Marian, *Annu. Rev. Phys. Chem.* **2021**, *72*, 617–640; c) H. Uoyama, K. Goushi, K. Shizu, H. Nomura, C. Adachi, *Nature* **2012**, *492*, 234–238; d) S. L. Murov, I. Carmichael, G. L. Hug, *Handbook of Photochemistry, 2nd ed.* CRC, New York, **1993**.

[3] a) S. Drouet, C. O. Paul-Roth, V. Fattori, M. Cocchic, J. A. G. Williams, *New J. Chem.* **2011**, *35*, 438–444; b) M. A. El-Sayed, *J. Chem. Phys.* **1963**, *38*, 2834–2838; c) M. Baba, *J. Phys. Chem. A* **2011**, *115*, 9514–9519.

[4] R. Englman, J. Jortner, *Mol. Phys.* **1970**, *18*, 145–164.

[5] a) A. Endo, K. Sato, K. Yoshimura, T. Kai, A. Kawada, H. Miyazaki, C. Adachi, *Appl. Phys. Lett.* **2011**, *98*, 083302; b) O. Yushchenko, G. Licari, S. Mosquera-Vazquez, N. Sakai, S. Matile, E. Vauthey, *J. Phys. Chem. Lett.* **2015**, *6*, 2096–2100; c) P. Ganesan, J. Baggerman, H. Zhang, E. J. R. Sudhölter, H. Zuilhof, *J. Phys. Chem. A* **2007**, *111*, 6151–6156; d) X.-K. Chen, D. Kim, J.-L. Brédas, *Acc. Chem. Res.* **2018**, *51*, 2215–2224.

[6] a) P. J. Angiolillo, K. Susumu, H. T. Uyeda, V. S. Y. Lin, R. Shediac, M. J. Therien, *Synth. Met.* **2001**, *116*, 247–253; b) P. J. Angiolillo, H. T. Uyeda, T. V. Duncan, M. J. Therien, *J. Phys. Chem. B* **2004**, *108*, 11893–11903.

[7] a) T. V. Duncan, K. Susumu, L. E. Sinks, M. J. Therien, *J. Am. Chem. Soc.* **2006**, *128*, 9000–9001; b) E. J. Peterson, W. Qi, I. N. Stanton, P. Zhang, M. J. Therien, *Chem. Sci.* **2020**, *11*, 8095–8104.

[8] a) S. Tretiak, *Nano Lett.* **2007**, *7*, 2201–2206; b) S. Tretiak, C. Middleton, V. Chernyak, S. Mukamel, *J. Phys. Chem. B* **2000**, *104*, 4519–4528; c) S. Tretiak, S. Mukamel, *Chem. Rev.* **2002**, *102*, 3171–3212.

[9] a) S. Richert, G. Bullard, J. Rawson, P. J. Angiolillo, M. J. Therien, C. R. Timmel, *J. Am. Chem. Soc.* **2017**, *139*, 5301–5304; b) P. J. Angiolillo, V. S.-Y. Lin, J. M. Vanderkooi, M. J. Therien, *J. Am. Chem. Soc.* **1995**, *117*, 12514–12527; c) J. Park, P. Deria, M. J. Therien, *J. Am. Chem. Soc.* **2011**, *133*, 17156–17159; d) R. Shediac, M. H. B. Gray, H. T. Uyeda, R. C. Johnson, J. T. Hupp, P. J. Angiolillo, M. J. Therien, *J. Am. Chem. Soc.* **2000**, *122*, 7017–7033.

[10] a) C. A. Kent, D. Liu, L. Ma, J. M. Papanikolas, T. J. Meyer, W. Lin, *J. Am. Chem. Soc.* **2011**, *133*, 12940–12943; b) C. A. Kent, B. P. Mehl, L. Ma, J. M. Papanikolas, T. J. Meyer, W. Lin, *J. Am. Chem. Soc.* **2010**, *132*, 12767–12769; c) G. Lan, Z. Li, S. S. Veroneau, Y.-Y. Zhu, Z. Xu, C. Wang, W. Lin, *J. Am. Chem. Soc.* **2018**, *140*, 12369–12373; d) W. Zhan, H. Gao, Y. Yang, X. Li, Q.-L. Zhu, *Adv. Energy Sustainability Res.* **2022**, *3*, 2200004; e) W. A. Maza, S. R. Ahrenholtz, C. C. Epley, C. S. Day, A. J. Morris, *J. Phys. Chem. C* **2014**, *118*, 14200–14210; f) X. Li, J. Yu, D. J. Gosztola, H. C. Fry, P. Deria, *J. Am. Chem. Soc.* **2019**, *141*, 16849–16857; g) X. Li, J. Yu, Z. Lu, J. Duan, H. C. Fry, D. J. Gosztola, K. Maindan, S. Surendran Rajasree, P. Deria, *J. Am. Chem. Soc.* **2021**, *143*, 15286–15297; h) J. Yu, X. Li, P. Deria, *ACS Sustainable Chem. Eng.* **2019**, *7*, 1841–1854; i) S. Goswami, J. Yu, P. Deria, J. T. Hupp, *ACS Energy Lett.* **2021**, *6*, 848–853; j) C. Y. Lee, O. K. Farha, B. J. Hong, A. A. Sarjeant, S. T. Nguyen, J. T. Hupp, *J. Am. Chem. Soc.* **2011**, *133*, 15858–15861; k) H.-J. Son, S. Jin, S. Patwardhan, S. J. Wezenberg, N. C. Jeong, M. So, C. E. Wilmer, A. A. Sarjeant, G. C. Schatz, R. Q. Snurr, O. K. Farha, G. P. Wiederrecht, J. T. Hupp, *J. Am. Chem. Soc.* **2013**, *135*, 862–869.

[11] W. A. Maza, A. J. Haring, S. R. Ahrenholtz, C. C. Epley, S. Y. Lin, A. J. Morris, *Chem. Sci.* **2016**, *7*, 719–727.

[12] a) J. Yu, J. Park, A. Van Wyk, G. Rumbles, P. Deria, *J. Am. Chem. Soc.* **2018**, *140*, 10488–10496; b) J. Yu, R. Anderson, X. Li, W. Xu, S. Goswami, S. Surendran Rajasree, K. Maindan, D. A. Gómez-Gualdrón, P. Deria, *J. Am. Chem. Soc.* **2020**, *142*, 11192–11202; c) S. S. Rajasree, J. Yu, S. M. Pratik, X. Li, R. Wang, A. S. Kumbhar, S. Goswami, C. J. Cramer, P. Deria, *J. Am. Chem. Soc.* **2022**, *144*, 1396–1406.

[13] a) M. B. Smith, J. Michl, *Chem. Rev.* **2010**, *110*, 6891–6936; b) M. Hanna, A. Nozik, *Int. J. Appl. Phys.* **2006**, *100*, 074510.

[14] Commonly, E_{S_1} can be approximated as experimental $E_{0,0}$ values determined from the crossing point of their normalized lowest energy absorption and fluorescence spectra, and E_{T_1} can be approximated from the phosphorescence peak. Alternatively, these energies can be obtained from TDDFT computations: E_{S_1} and E_{T_1} for H_4TBAPy are 2.96 and 1.79 eV;

for NU-1000 are 2.91 and 1.61 eV; for H_4PEPF are 3.20 and 2.07 eV; and for SIU-100 are 3.31 and 2.09 eV.
[15] Y. J. Bae, G. Kang, C. D. Malliakas, J. N. Nelson, J. Zhou, R. M. Young, Y.-L. Wu, R. P. Van Duyne, G. C. Schatz, M. R. Wasielewski, *J. Am. Chem. Soc.* **2018**, *140*, 15140–15144.
[16] D.-G. Ha, R. Wan, C. A. Kim, T.-A. Lin, L. Yang, T. V. Voorhis, M. A. Baldo, M. Dincă, *Nat. Mater.* **2022**, *21*, 1275–1281.
[17] In terms of triplet quenching, but may involve photo-induced electron transfer producing oxygen radical anion.
[18] P. Deria, J. Yu, T. Smith, R. P. Balaraman, *J. Am. Chem. Soc.* **2017**, *139*, 5973–5983.
[19] a) J. Park, M. Xu, F. Li, H.-C. Zhou, *J. Am. Chem. Soc.* **2018**, *140*, 5493–5499; b) J. M. Rowe, J. Zhu, E. M. Soderstrom, W. Xu, A. Yakovenko, A. J. Morris, *Chem. Commun.* **2018**, *54*, 7798–7801.
[20] Deposition number 2216519 (for SIU-175) contains the supplementary crystallographic data for this paper. These data are provided free of charge by the joint Cambridge Crystallographic Data Centre and Fachinformationszentrum Karlsruhe Access Structures service.
[21] P. Deria, D. A. Gómez-Gualdrón, W. Bury, H. T. Schaef, T. C. Wang, P. K. Thallapally, A. A. Sarjeant, R. Q. Snurr, J. T. Hupp, O. K. Farha, *J. Am. Chem. Soc.* **2015**, *137*, 13183–13190.
[22] Solvent-accessible porosity was probed via thermogravimetric analysis (TGA) of the respective DMF-filled MOF sample, showing an initial mass loss of ≈87 % associated with the evaporation of the solvent filled within the MOF pores; (see Supporting Information sec C3).
[23] M. Mitsui, Y. Kawano, R. Takahashi, H. Fukui, *RSC Adv.* **2012**, *2*, 9921–9931.
[24] a) P. Deria, W. Bury, J. T. Hupp, O. K. Farha, *Chem. Commun.* **2014**, *50*, 1965–1968; b) P. Deria, J. E. Mondloch, E. Tylianakis, P. Ghosh, W. Bury, R. Q. Snurr, J. T. Hupp, O. K. Farha, *J. Am. Chem. Soc.* **2013**, *135*, 16801–16804; c) A. Van Wyk, T. Smith, J. Park, P. Deria, *J. Am. Chem. Soc.* **2018**, *140*, 2756–2760.
[25] Formed from higher energy singlets at the early time (< 1 ns) and appears at the same proportion as found in pristine MOF and were not quenched by atRA or O_2; this signal is associated with low-energy "trapped" state formed at the imperfection sites of the crystals.
[26] Emission from the initial S_1S_0 pair appears *ca* 525 nm; alternatively, the $S_1 \rightarrow S_0$ emission appears at ≈580 nm and at a longer time delay. Considering the fast timescale for this SF-mediated formation of ^{1}(TT) state, an alternate possibility can be considered where the population is condensed to a specific/selective vibrational state. For that case, however, the spontaneous emission envelope would be narrow and centered around 550 nm and would not show the time-resolved profile described in Figure . Condensing the S_1–S_0 transition probability to one of the vibrational levels of the S0 state that is not spontaneous will be very unusual.
[27] K. T. Munson, J. Gan, C. Grieco, G. S. Doucette, J. E. Anthony, J. B. Asbury, *J. Phys. Chem. C* **2020**, *124*, 23567–23578.
[28] C. E. Miller, M. R. Wasielewski, G. C. Schatz, *J. Phys. Chem. C* **2017**, *121*, 10345–10350.
[29] T. C. Berkelbach, M. S. Hybertsen, D. R. Reichman, *J. Chem. Phys.* **2013**, *138*, 114103.
[30] a) R. R. Islangulov, D. V. Kozlov, F. N. Castellano, *Chem. Commun.* **2005**, 3776–3778; b) T. N. Singh-Rachford, F. N. Castellano, *J. Phys. Chem. Lett.* **2010**, *1*, 195–200; c) M. Adams, M. Kozlowska, N. Baroni, M. Oldenburg, R. Ma, D. Busko, A. Turshatov, G. Emandi, M. O. Senge, R. Haldar, C. Wöll, G. U. Nienhaus, B. S. Richards, I. A. Howard, *ACS Appl. Mater. Interfaces* **2019**, *11*, 15688–15697.
[31] This resolved spectrum is caused due to a diminished 580 nm peak that was highly intense in the unmodified SIU-175 (caused via reverse populated via TTA) and somewhat quenched possibly via energy transfer to TPP(Pd) whose absorption band spans from 520–600 nm.

Manuscript received: April 18, 2023
Accepted manuscript online: July 31, 2023
Version of record online: August 8, 2023